Applied Thermal Engineering 112 (2017) 1510–1522

Contents lists available at ScienceDirect

Applied Thermal Engineering

journal homepage: www.elsevier.com/locate/apthermeng

Research Paper

A methodology for thermal analysis of complex integrated systems: Application to a micro-CHP plant

Jorge E.P. Navalho *, José M.C. Pereira, José C.F. Pereira

LAETA, IDMEC, Instituto Superior Técnico, Universidade de Lisboa, Lisboa, Portugal

HIGHLIGHTS

- A methodology for thermal analysis of complex multi-component systems is presented.
- The methodology is verified for a particular system with different boundary conditions.
- The methodology is applied to investigate the thermal performance of a μ-CHP unit.
- Critical hot-spots are observed on the external surface of the unit components.
- Thermal management studies can take advantage of the current thermal analysis methodology.

GRAPHICAL ABSTRACT

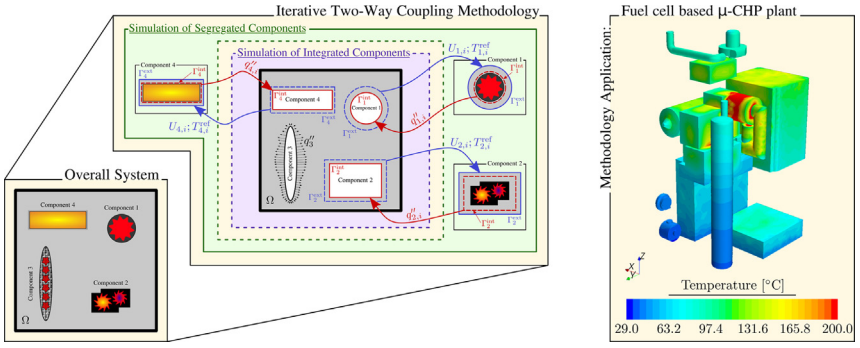

ARTICLE INFO

Article history:
Received 16 May 2016
Revised 23 October 2016
Accepted 31 October 2016
Available online 1 November 2016

Keywords:
Thermal analysis
Thermal management
Integrated components
μ−CHP system
Hot-spots
Heat transfer

ABSTRACT

Thermal analysis and management studies are commonly conducted from early design stages of new products by numerical means. However, the application of three-dimensional tools for evaluating the thermal performance of multi-component systems, exhibiting high geometrical and phenomenological complexities may become unpractical in view of the long computational times. Therefore, a methodology for thermal analysis of complex thermal systems is developed to improve the overall numerical convergence rate. The methodology is based on an iterative two-way coupling procedure between two sets of simulations: simulation set where critical components are individual and fully simulated (component-level simulations); and simulation framework where the overall system is considered with hollow components (system-level simulation). A communication strategy between both simulation sets is established. The methodology can be readily applied for performing thermal management studies. A verification procedure for the suggested methodology is firstly carried out. Afterwards, the methodology is applied to investigate the thermal performance at the system-level of a fuel cell based μ−CHP unit, namely regarding the feasibility of components integration. The methodology application allowed the identification of critical hot-spots (with temperatures up to about 400 °C) on the surface of the unit internal components, mainly due to an inadequate insulation thickness and shape.

1. Introduction

Thermal management has become a common concern from early design stages of many integrated systems developed in the fields of electrical or mechanical engineering. In particular, thermal

* Corresponding author.
E-mail address: jorge.navalho@tecnico.ulisboa.pt (J.E.P. Navalho).

http://dx.doi.org/10.1016/j.applthermaleng.2016.10.201
1359-4311/

Nomenclature

$\mathbf{x}$	local position along physical boundaries or auxiliary interfaces
e^{FS}	relative error in relation to the full simulation solution
h	convection heat transfer coefficient
i (i_{total})	iteration (total number of iterations)
k	thermal conductivity
q''	heat flux
T	temperature
U ($\overline{U}$)	local (global) overall heat transfer coefficient

Greek letters

α_k	iteration termination tolerance for component k
Γ_k^{ext} (Γ_k^{int})	external (internal) boundary/interface of component k

Superscripts and subscripts

ref	reference
i	iteration
k	component k

Acronyms

CAD	computer-aided design
CFD	computational fluid dynamics
CHP	combined heat and power

analysis has been considered for the development of power converters [1,2], battery modules [3,4], electrical machines [5] and compact (high-power density) electronic equipments, such as LED (light emitting diode) based applications [6–8] or mobile devices [9,10]. In the automotive industry, the vehicle underhood has been considered a subject of intensive investigation regarding thermal management issues [11,12]. The interest in performing thermal analysis studies during the product development cycle has been driven by the increasing trends for energy efficiency, cost reduction, miniaturization, safety, product reliability and high performance [13,5,14]. Thermal diagnosis during the product development phase allows for the determination of hot-spots and severe temperature gradients within the system. Therefore, improved prototypes with different packaging configurations or different materials can be developed considering the outcome from thermal analysis.

Thermal design studies can be carried out experimental, theoretical and numerically. However, an increasing application of computational tools to predict the thermal behavior of new products has been observed, mainly due to the shrinking time-to-market for new products combined with the high cost of prototypes for experimental testing and the increasingly available computing power [14,11,15].

The application of computational tools, namely CFD (computational fluid dynamics) methods allows for the full evaluation of heat transfer in systems composed simultaneously by solid and fluid phases and, consequently, for the determination of temperature distribution maps in the whole system. However, depending on the geometrical and phenomenological complexity of the system under consideration, the full solution by CFD methods can become prohibitive. For this reason, several strategies have been proposed in an attempt to harmonized the accurate predictability generally attributed to CFD methods with a reasonable computational workload. Several authors have solved the fluid flow mass, momentum and energy equations iteratively with the energy equation of the solid domain for determining the aero-thermal performance of engine compartments [16,17]. For evaluating the underhood thermally driven flow during thermal soak (transient regime), a strategy was proposed based on a sequence of "unfrozen/frozen" steps for solving the mass and momentum fluid flow equations, while the solid and fluid energy equations advance continuously in time [18]. To alleviate the CFD task while taking into account the performance of liquid cooling systems in the calculation of the air behavior around underhood components and inside the passenger cabin, 3D (three-dimensional) CFD models have been generally combined with 1D (one-dimensional) thermo-fluid models to represent the coolant path [19,11]. Other works have considered flow network models with lumped parameters (characteristic curves) obtained by prior CFD application (model reduction) for underhood thermal analysis [20] and to evaluate the performance of the cooling system for power electronics in fuel cell vehicles [21].

Micro-combined heat and power (μ–CHP) systems are examples of highly complex thermal equipment. These systems constitute a promising technology to produce electrical and thermal energy from a single energy feedstock, at the energy consumption site and with high overall (combined) efficiency [22,23]. Among the different fuel conversion technologies commonly considered for μ–CHP systems, the electrochemical fuel conversion with fuel cells offers a more efficient and cleaner fuel conversion path towards electricity and heat, with low noise levels and simple maintenance requirements [23,24]. In particular, solid oxide fuel cells have been widely considered for micro-cogeneration systems due to the fuel flexibility, the capability for internal fuel reforming and the CO tolerance [25,24]. Although μ–CHP systems have been extensively investigated, namely concerning the economic feasibility and environmental advantages [26,27], and system design (performance) studies [28–31], as far as the authors are aware, no comprehensive thermal analysis study on the components integration into a fuel cell based μ–CHP plant has been reported in the open literature.

The current work presents a methodology for thermal analysis of geometrical and phenomenologically complex systems composed by an arbitrary number of integrated components, each one having a specific thermal footprint in the system. The methodology provides an alternative convergence pathway for the numerical solution of complex problems in relation to the conventional simulation approach. After conducting a verification procedure, the methodology is applied to predict the thermal performance of a fuel cell based μ–CHP plant developed for supplying heat and electricity in a decentralized (distributed) scenario.

The manuscript is organized as follows: Section 2 provides a detailed description of the methodology, which is verified for a specific system in Section 3 and, finally, applied to a μ–CHP plant in Section 4. Summary conclusions are presented in Section 5.

2. Proposed methodology

The current methodology divides the global problem into two independent sets of simulations: (1) simulation of segregated components (component-level simulations); and (2) simulation of integrated components (system-level simulation). These two sets of simulations communicate with each other through a two-way coupling procedure. In the simulation of integrated components, the overall system is considered with hollow components. This means that the components are located in the respective installation sites

but the interior of each component, as well as all the phenomena that therein occurs are completely neglected. The net heat release from components with an unknown thermal footprint on the overall system is iteratively calculated at the simulation of segregated components level and exported to the simulation of integrated components framework. At the simulation of segregated components level, each component is individual and fully simulated apart from other components but taking into account their thermal interactions in the overall system.

The application of the methodology embraces two stages in the following order: (1) problem definition; and (2) iterative two-way coupling procedure. The problem definition stage starts by realizing which components comprising the system should be fully simulated, *i.e.*, which components require the solution of the balance equations that govern their internal phenomenological processes, in order to determine their heat release to the surrounding environment. Consequently, these components are taken into account in the simulation of segregated components set. The problem definition stage ends up by defining fictitious (auxiliary) surfaces enclosing each selected component for full simulation. These surfaces are simultaneously required to define the computational domains at both simulation levels and to couple both simulation sets.

Fig. 1 depicts the application of the methodology to an illustrative and generic system. This figure portrays particularly the problem definition stage and the data fluxes coupling both simulation sets that are evaluated according to the iterative two-way coupling approach. Although the methodology does not dictate a maximum limit for the number of components, for simplicity, the system under consideration is composed only by four generic components whose internal operation affects the thermal performance of the whole system. The actual processes taking place within each component are not relevant to illustrate the methodology application. Besides the four components, the system domain (Ω) can be composed by solid and fluid regions.

Starting by the problem definition stage, consider that the thermal effect of Component 3 on the system is found to be fully characterized by a particular heat flux distribution on its external boundary (q''_3), whereas the heat load from the remaining components is unknown. Therefore, detailed (full) simulations are addressed only for the Components 1, 2 and 4. Proceeding with the problem definition stage, two fictitious surfaces are arbitrarily established around each component ascribed for full simulation (see in Fig. 1 the Surfaces Γ_k^{ext} and Γ_k^{int} represented by blue and red lines, respectively, around the Components 1, 2 and 4). These two surfaces have to be defined within a solid region or at a fluid/solid interface, must encompass the component, and should not be coincident for improving the convergence rate and the robustness of the methodology. In fact, the experience revealed that using the same boundary should be avoided, namely for cases where components simultaneously receive and release heat. The external (internal) surface corresponds simultaneously to a physical boundary in the simulation of segregated (integrated) components and to an auxiliary interface in the simulation of integrated (segregated) components. According to the current two-way coupling procedure, data is evaluated along auxiliary interfaces (dashed lines around each component in Fig. 1) in order to be transported and imposed on physical boundaries (solid lines around each component in Fig. 1).

The next stage consists in the application of the iterative two-way coupling procedure whose sequence of steps is depicted in Fig. 2. The procedure starts by performing the numerical simulation for the governing equations and boundary conditions of each selected component for the simulation of segregated components set. This set of simulations is carried out considering for the energy equation the boundary condition described by Eq. (1) at the components' external boundary (Surfaces Γ_k^{ext}). In Eq. (1), $\mathbf{n_k}$ is the unit outward normal vector to the external surface of component k, and $U_{k,i}$ and $T_{k,i}^{ref}$ correspond to the local overall heat transfer coefficient and reference temperature, respectively, along the Surface Γ_k^{ext} at the iteration i.

$$-(k\nabla T\cdot\mathbf{n_k}) = U_{k,i}\left[T\left(\Gamma_k^{ext}\right) - T_{k,i}^{ref}\right] \tag{1}$$

Initially (iteration 0 – initialization step, see Fig. 2), a global value for the overall heat transfer coefficient ($\overline{U}_k$) can be estimated based on several geometrical and thermophysical parameters of

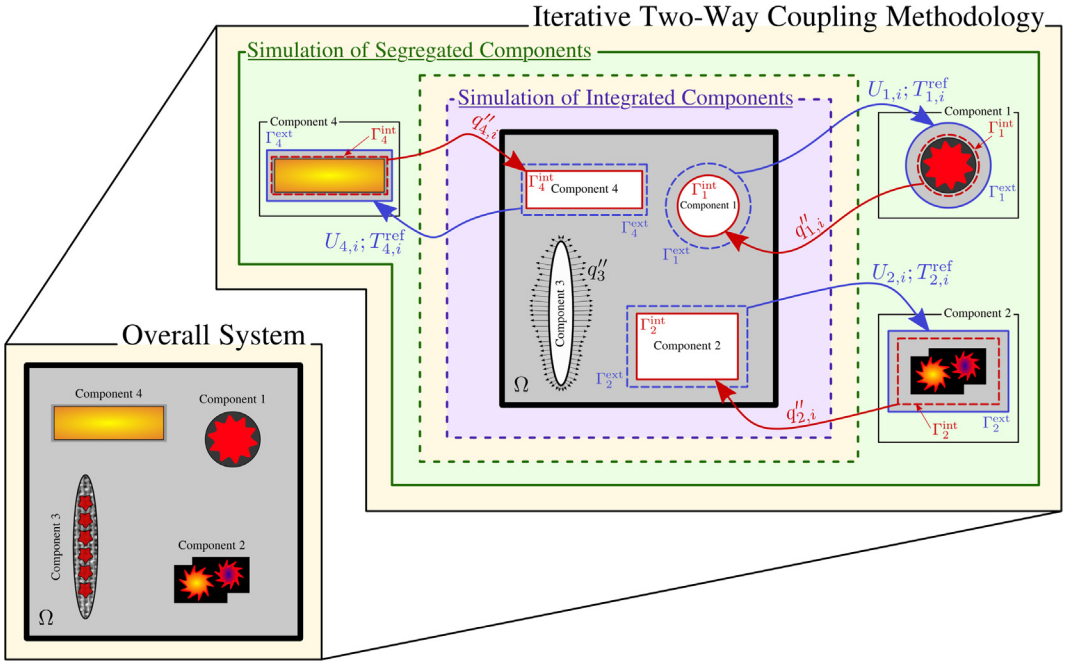

Fig. 1. Schematic representation of the iterative two-way coupling methodology applied to a generic system composed by four components.

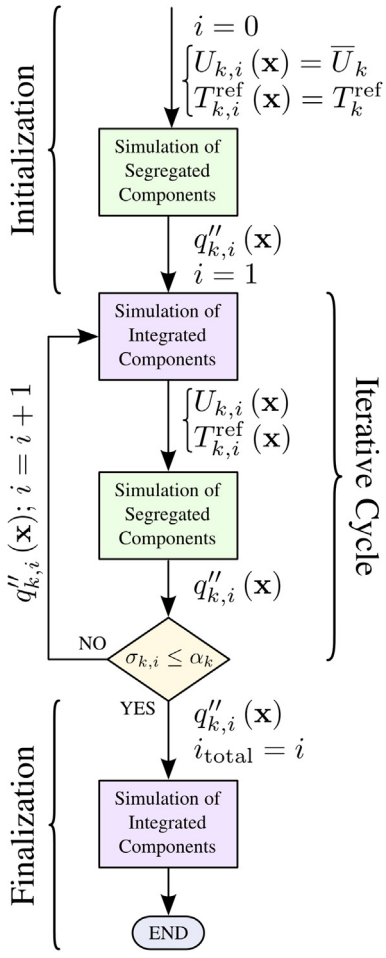

Fig. 2. Flow chart of the proposed iterative two-way coupling methodology.

the overall system (considering a one-dimensional heat transfer approximation) or through preliminary simulations. However, a rough guess for the overall heat transfer coefficient can be considered without a significant penalization on the iterative convergence rate of the methodology. For instance, a specific convection heat transfer coefficient value around the component can be readily considered as an initial guess. The reference temperature can be assigned to the external (environment) system temperature. After a converged solution is achieved for all components, the heat flux distribution along the auxiliary interface (Surface Γ_k^{int}) of each component ($q''_{k,0}$) is computed and stored, and the initialization step is over.

The step that follows corresponds to the first phase of the iterative procedure itself (iterative cycle – see Fig. 2). For any iteration, the iterative cycle starts at the simulation of integrated components level by mapping the stored heat flux distributions ($q''_{k,i}$) on the physical boundary of each component (Surface Γ_k^{int}). After performing the numerical simulation for the whole system with hollow components, the local overall heat transfer coefficients for each component are computed on the auxiliary interfaces (Surfaces Γ_k^{ext}) through the Eq. (2) based on specific reference temperatures.

$$U_{k,i} = \frac{\mathbf{q''_{k,i}} \cdot \mathbf{n_k}}{\left[T(\Gamma_k^{\text{ext}}) - T^{\text{ref}}_{k,i}\right]} \tag{2}$$

If in any location along the Surface Γ_k^{ext} the dot product $\mathbf{q''_{k,i}} \cdot \mathbf{n_k}$ becomes negative it implies that the component k will receive thermal energy from the surrounding environment through such location. In this case, the reference temperature should be assigned to an arbitrary high value to compute the local overall heat transfer coefficient. Therefore, two reference temperatures should be considered: one representative of the lower and other representative of the higher temperatures. The reference temperature representative of lower (higher) temperatures should be lower (higher) than the lowest (highest) temperature observed along the iterative sequence of the methodology. The actual values considered for the reference temperatures do not affect the final solution because these values correspond to internal and auxiliary values of the iterative cycle. Nevertheless, the values considered for the reference temperatures have to assure a non-zero result for the denominator of Eq. (2). This formalism allows for the thermal interaction (thermal coupling) between fully (and independently) simulated components, in such a way that each component can simultaneously release and receive heat through different but well defined surfaces.

After computing the distributions of the overall heat transfer coefficients and defining the reference temperatures for all selected components, the current iteration continues at the simulation of segregated components level for determining the heat flux distribution on the auxiliary interfaces (Surfaces Γ_k^{int}) of each fully simulated component in a similar manner as previously described for the initialization step. The actual iteration terminates by evaluating for every component the compliance with a specific criterion ($\sigma_{k,i} \leqslant \alpha_k$) taking into account an established iteration termination tolerance (α_k). Although different stopping criteria can be considered, in the current methodology formulation $\sigma_{k,i}$ is based on the heat flux distributions for each fully simulated component obtained in the actual and previous iterations (iterations i and $i-1$, respectively), according to Eq. (3).

$$\sigma_{k,i} = \frac{\int \left(q''_{k,i} - q''_{k,i-1}\right) dA}{\int q''_{k,i} dA} \tag{3}$$

If the criterion is not satisfied for at least one component the iterative procedure is repeated, *i.e.*, a new iteration (iteration $i+1$) is performed but with a better guess for the heat flux distributions that was obtained during the previous iteration (iteration i). The iterative stage of the methodology comes to the end when the iteration termination criterion is respected for all components.

The methodology is concluded by performing the simulation for the overall system, at the simulation of integrated components level, taking into account the heat flux distribution for each component derived during the last iteration of the procedure. This operation constitutes the finalization stage of the methodology (see Fig. 2). The application of the methodology with a sufficiently low iteration termination tolerance for each component allows to achieve an equivalence between the solution obtained in both sets of simulations and the solution that would be attained with a full simulation (complete simulation in one simulation environment) for the overall system.

Variations of the current methodology can be readily formulated based on different methods for data mapping between simulation sets, based on different strategies to account for the possibility of a component to simultaneously receive and release heat, or based on different criteria for the termination of the iterative procedure. In particular, to alleviate the coupling process, instead of local heat fluxes and local overall heat transfer coefficients, global values can be considered suitable for specific cases. Moreover, even though the current methodology is formulated for steady-state applications, a variation for unsteady conditions can be immediately developed by assuming a quasi-stationary state between both sets of simulations.

The application of the present methodology contributes to an increase in the convergence rate of the overall numerical solution, namely for geometrically complex systems containing several components, each one governed by specific and independent phenomena with significantly different characteristic time/length scales. This is because each component considered for full simulation is simulated in an independent environment, where the numerical stiffness can be reduced, appropriate numerical models can be applied, and more suitable meshes can be considered. Furthermore, this methodology can be exploited for thermal management studies since it supports an automation for the design workflow of new products (enhancing the productivity) in two possible fashions: (1) the methodology allows for an independent development of a specific component, while the remaining system (components, support structures, *etc.*) remains fixed and "waiting" for an improved design configuration of the component under development; and (2) once the system components design is closed, the current methodology can be applied systematically for determining better positions within the overall system to install the components, in such a way that the heat management in the system is enhanced. The advantages of using the current methodology for the two possible scenarios are related with the fact that the tedious and time-consuming process related with CAD (computer-aided design) modeling and mesh generation of the whole system is avoided, whenever an improved component design is to be integrated in the system (Case (1)), or the components location in the system is shuffled (Case (2)).

3. Methodology verification

This section provides a comparison between the results from the application of the present methodology and the results obtained by the full simulation approach – simulation of the overall system in the same simulation environment. The 2D (two-dimensional) system presented in Fig. 3(a) is considered for this purpose. The system consists of two components enclosed by an insulating material. Component 1 corresponds to a gas passageway where a specific gas stream (aligned with the positive *x*-axis) enters at 350 K and is heated in the last half part of the container. The upstream and downstream manifolds of Component 1 were not considered for system simplification. Component 2 has a semi-circular shape whose external boundaries are defined by the Surfaces 9 and 10. The thermal performance of the Component 2 is fully characterized by a particular heat flux distribution on its external surfaces. Therefore, according to the current methodology only Component 1 is considered in the simulation of segregated components framework. The boundary conditions applied along the eight external surfaces of the overall system are presented in Fig. 3(a). Different types of boundary conditions (Dirichlet, Neumann, convection) were purposely considered to demonstrate the robustness of the methodology.

The methodology is applied considering two cases based on the heat flux prescribed on the semi-circular boundary of Component 2 (Surface 9). In Case I, Surface 9 is considered an adiabatic wall ($q''_9 = 0\ \mathrm{W\,m^{-2}}$), while in Case II an heat flux towards the insulation equal to 250 W m^{-2} is imposed. These two cases intend to promote proper conditions to observe different thermal behaviors between Component 1 and the remaining system. In Case I, Component 1 will only release heat to the surrounding environment, whereas in Case II, Component 1 is expected to simultaneously release and receive heat from the system where it is integrated.

The auxiliary interfaces for Component 1 (Surfaces Γ_1^{ext} and Γ_1^{int}) are presented in Fig. 3(a). The internal surface encloses the Component 1 (gas and gas container), whereas the external surface encompasses the Component 1 and a portion of the insulating material. Fig. 3(b) presents the system regions (computational domains) considered in the two simulation frameworks, according to the current methodology. The system regions considered in each simulation set are defined in agreement with the fictitious interfaces established in Fig. 3(a).

The commercial software package STAR-CCM+ (a finite volume based CFD solver developed by CD-Adapco) was used to obtain the solution of the temperature field in the whole system for both case studies, considering the full simulation approach and the application of the current methodology. For both case studies, the initialization step required by the methodology (see Fig. 2) was started by assuming for Component 1 a constant (spatially independent – global) overall heat transfer coefficient ($\overline{U}_1$) equal to 40 W m^{-2} K^{-1} and a reference temperature (T_1^{ref}) of 300 K. The assigned reference temperature implies an energy loss all around

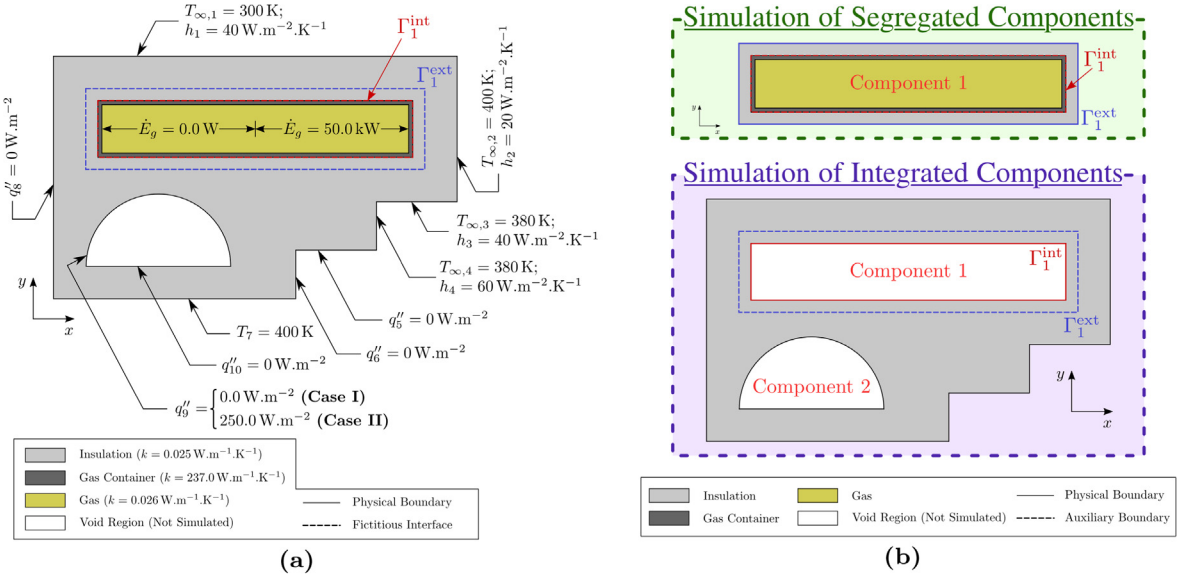

Fig. 3. System considered for the methodology verification: (a) whole system and boundary conditions; (b) decomposition of the overall system into the regions considered for each simulation set (simulation of segregated components and simulation of integrated components).

the component external boundary because this temperature value is lower than the minimum temperature expected within the component.

Figs. 4(a) and (b) present several convergence performance parameters evaluated at both simulation levels along the iterative process, for the two cases under consideration. In particular, Fig. 4 (a) shows the error of the actual net heat transfer rate (through the internal auxiliary interface) in relation to the previous value ($\sigma_{1,i}$ – see Eq. (3)) and in relation to the full simulation value ($e^{FS}_{1,i}$). Fig. 4(b) shows the net heat transfer rates ($q'_{1,i}$) and the outlet average gas temperatures within Component 1 ($\overline{T}^{gas,out}_{1,i}$). A total of eight and 18 iterations were considered for Case I and Case II, respectively.

Both relative errors ($\sigma_{1,i}$ and $e^{FS}_{1,i}$) decrease along the iterative procedure as Fig. 4(a) shows. This decreasing behavior is more remarkable for Case I, according to which the component independently simulated does not receive energy through any location along its boundary. On the contrary, for Case II the Component 1 that was considered at the initialization step (iteration 0) a purely dissipative component has to adapt, as the iterative procedure evolves, to the situation of receiving energy through an increasing portion of its boundary. For this reason, a higher number of iterations is observed for Case II in relation to Case I, in order to achieve the same convergence criterion (same values for $\sigma_{1,i}$ or $e^{FS}_{1,i}$). An acceleration towards the required tolerance for Case II can be pursued at the cost of providing a more accurate guess for the overall heat transfer coefficients and reference temperatures at the initialization stage.

As a consequence of the rough estimation provided for $\overline{U}_1$ and T^{ref}_1 for both case studies, the component considered for full simulation releases more energy than that expected through the full simulation of the system. In particular, as Fig. 4(b) supports, at the end of iteration 0 the Component 1 in Case I and II loses about 3.84 and 4.87 times more energy, respectively, than the final values obtained with the iterative procedure (that correspond to the values attained by the full simulation). Moreover, in full agreement with the higher values predicted for the net heat release, the outlet average gas temperatures for both case studies are lower than the expected (final) values. For Case II, the prescribed heat release from Component 2 was responsible for decreasing the net heat release from Component 1 to the surrounding environment in relation to Case I. Therefore, in accordance with the fact that Component 1 also receives energy from other components of the system, the outlet average gas temperature at the end of the iterative procedure is slightly higher for Case II in relation to Case I.

Figs. 5(a) and (b) present for Case I and Case II, respectively, the development of the temperature solution along the iterative procedure for the system region considered in the simulation of integrated components. In agreement with the convergence analysis presented in Fig. 4(a), Case I requires less iterations to converge. Particularly, from three iterations for Case I and 15 iterations for Case II minor temperature deviations are observed. As a consequence of the starting estimate for Case II, Fig. 5(b) shows high temperatures between Components 1 and 2, especially, for the solutions obtained with one to three iterations. Nevertheless, as the iterative procedure advances the temperature in this region decreases due to the fact that Component 1 starts to receive energy from Component 2.

Figs. 6(a) and (b) report the temperatures in the overall system for both case studies obtained through the full simulation approach and through the current methodology, respectively. An iteration termination tolerance (α_1) equal to 1.0×10^{-3} was considered for the stopping criterion of the iterative procedure. According to Fig. 4(a), this tolerance was achieved within only three iterations (i_{total}) for Case I and 15 iterations for Case II. No striking differences can be drawn between the results from both approaches and, consequently, a general good matching is addressed comparing the results of the full simulation approach and the current methodology for both case studies. This evidence strongly supports the validity of the proposed methodology for thermal analysis of complex systems.

4. Application of the methodology to a μ–CHP plant

The methodology presented and verified previously is herein applied to analyze the steady-state thermal performance of a fuel cell based μ–CHP unit that was developed for supplying electrical power and heat in a domestic context. The system is composed by several components with a complex geometrical arrangement within the unit. In particular, the interest in this application relies on evaluating the external temperature of the unit, in order to

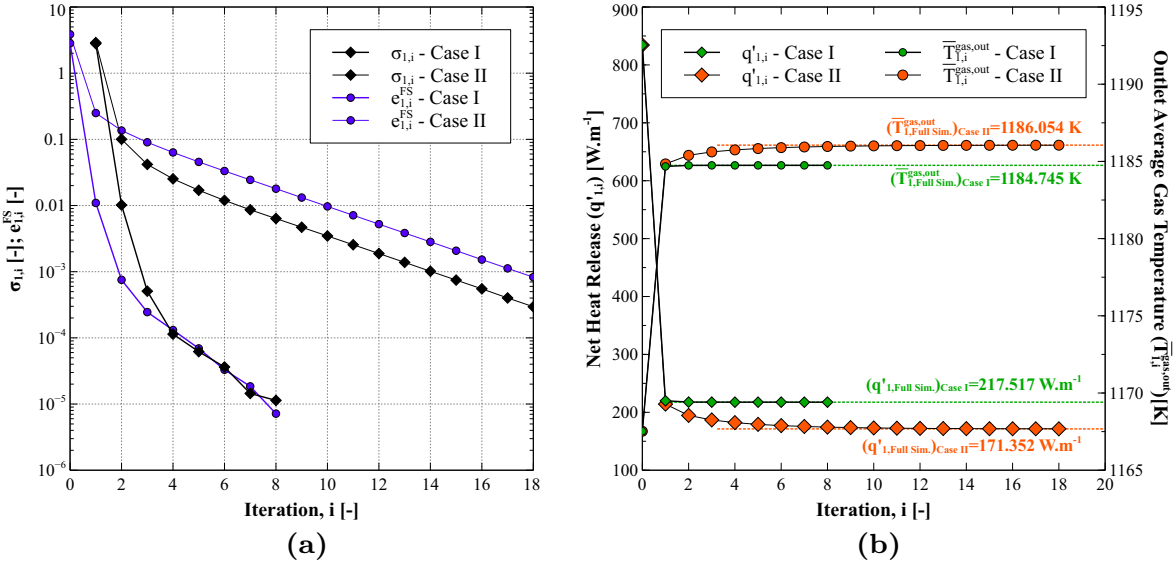

Fig. 4. Progression of the iterative procedure for Case I and Case II: (a) errors registered at each iteration in relation to the previous iteration ($\sigma_{1,i}$) and in relation to the full simulation solution ($e^{FS}_{1,j}$); (b) net heat release from Component 1 and outlet average gas temperature.

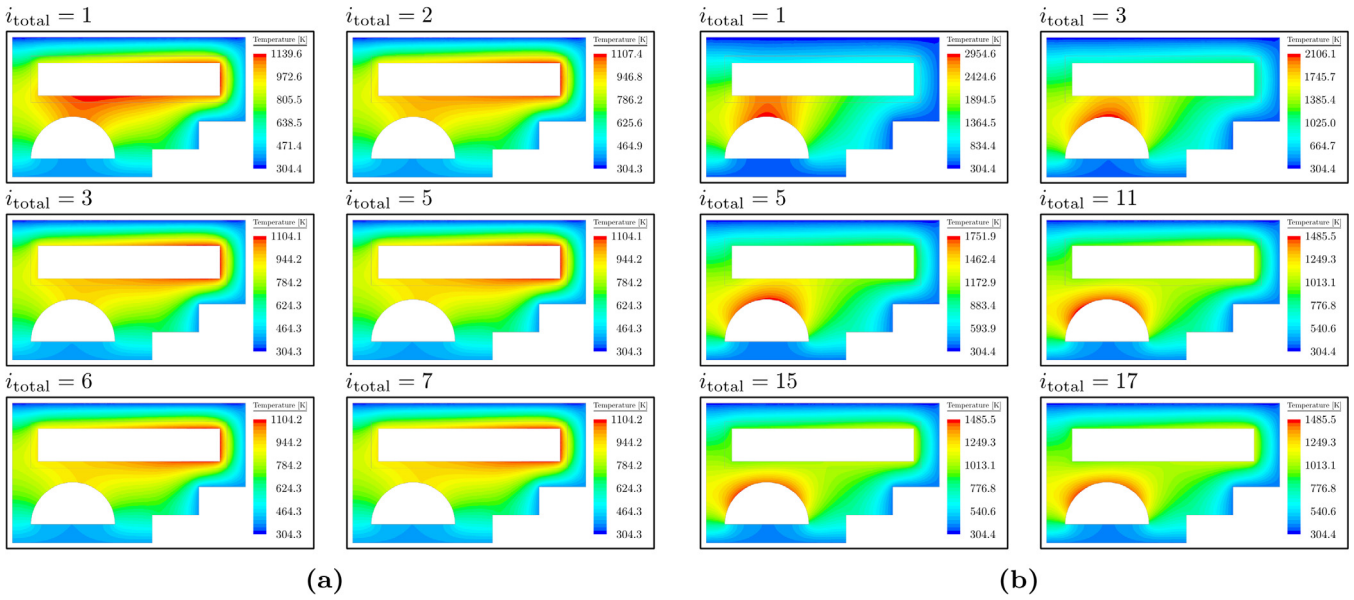

Fig. 5. Evolution of temperatures with the total number of iterations in the system domain considered for the simulation of integrated components: (a) Case I; (b) Case II.

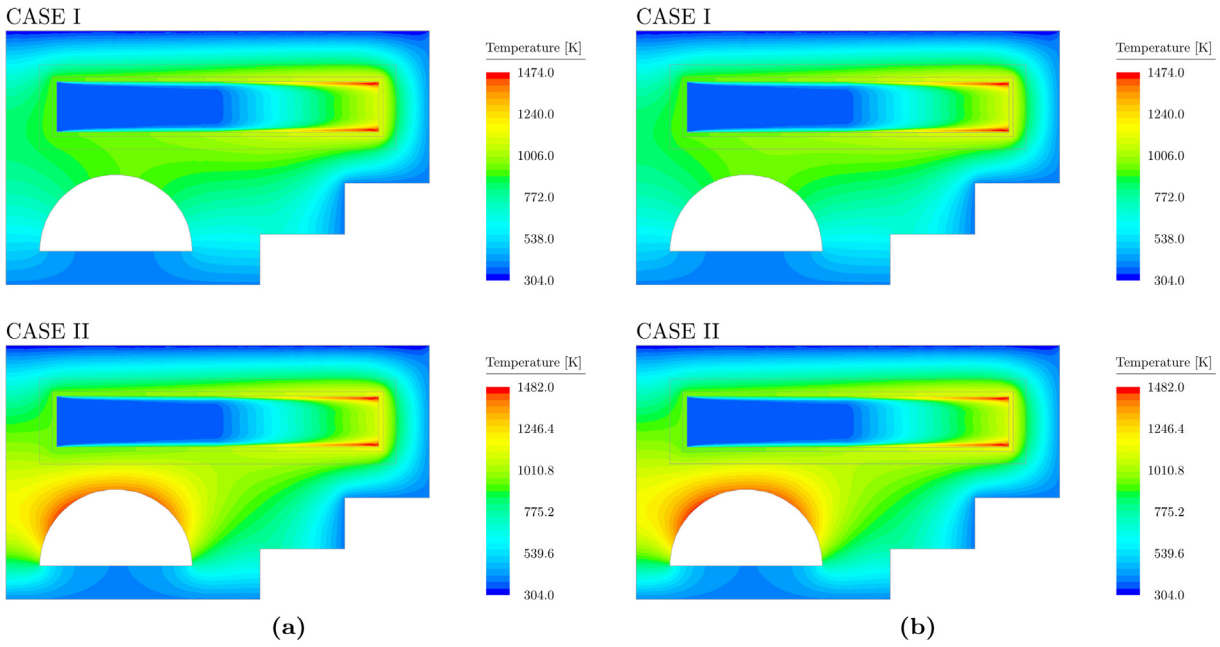

Fig. 6. Temperatures in the whole system for Case I and Case II computed through: (a) full simulation approach; (b) current methodology with an iteration termination tolerance of 1.0×10^{-3}.

demonstrate the feasibility of components integration in the system.

4.1. Fuel cell based μ−CHP plant: main components and overall description of operation

Fig. 7 presents a schematic representation for the key components of the μ−CHP unit under consideration, as well as the relationship among these components. A global description on the unit operation including the role played by each unit component is provided as follows. An hydrocarbon fuel stream (natural gas or biogas mixtures) after a desulphurization stage (along the desulphurizer – Component 1) is mixed with air in a static mixer (Component 2). This mixture is heated along the reformer gas preheater (heat exchanger – Component 3) and fed to the reformer (Component 4) where the partial oxidation of the air/fuel mixture takes place (in a catalyst honeycomb monolith bed) for synthesis gas (mixture of H_2 and CO) generation. The reformate mixture is thereafter provided to the anode inlet of the solid oxide fuel cell stack (Component 5). The surplus H_2 content, as well as the CO stream from the anode fuel cell off-gas are fully oxidized in the afterburner (Component 6). The sensible heat of the burner exhaust gas is recovered along three successive heat exchangers, prior to the exhaust gas release into the atmosphere: the cathode air preheater (Component 7), the reformer gas preheater (Component 3) and, finally, the water heater (Component 8) where the useful thermal output from the unit is generated. During transients, namely in the start-up regime, the cathode air stream required for fuel cell operation is heated in an electrical air

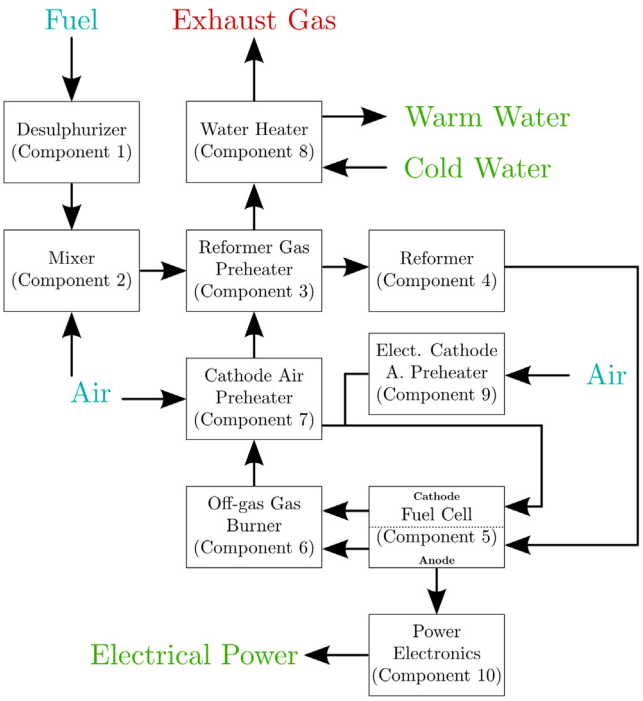

Fig. 7. Schematic process diagram of the μ–CHP unit.

preheater (Component 9). This is due to the poor heat content of the exhaust gas from the burner, that is insufficient to increase the cathode air temperature to the required values. The electrical power generated in the fuel cell stack is controlled and delivered to external electrical grid by the power electronics unit (Component 10) that is essentially composed by an inverter and a control system. A complementary description on the μ-CHP system features can be found elsewhere [32].

For numerical simulation purposes, Fig. 8 presents the computational room where the unit was placed, the external geometry of the unit, the main components affecting its thermal performance and the components location within the unit. The most critical components due to its high thermal power were placed within an insulated block (see "Insulated Components" in Fig. 8). A ventilated room for the unit installation was considered to avoid the need of applying specific boundary conditions directly on the external unit surfaces. The CAD model of the unit was subjected to a geometry cleanup (defeaturing) process for the elimination of irrelevant (minor) features that do not critically affect the heat transfer and fluid flow behavior. This initial stage for geometry simplification becomes of paramount importance for the successful preparation of the computational representation (mesh generation) of the unit, as well as for decreasing the computational labor for achieving a converged solution. CAD modeling (defeaturing) and mesh generation were carried out with the software package STAR-CCM+.

4.2. Segregated components framework

According to the proposed methodology, three fundamental components were considered for full simulation (in the simulation of segregated components framework). These critical components correspond to the reformer gas preheater, the reformer and the anode off-gas burner. Figs. 9(a) to (c) present the mesh geometry for these components.

The reformer gas preheater consists of a compact plate-type heat exchanger with the function of increasing the reformer inlet gas temperature at the expense of the heat content of the flue gases from the burner (see "Component 3" in Fig. 7). Different meshes were developed for the solid and fluid regions taking into account conformal interfaces. For the solid phase a polyhedral mesh and the embedded thin mesher for the thin tubes were considered, whereas for the fluid region a combination of polyhedral cells with a prismatic layer on the walls was regarded, as well as mesh extruders for the inlet and outlet sections. The overall mesh for the reformer gas preheater presented in Fig. 9(a) is composed by approximately 4.5 million cells. The fresh reactive mixture enters through the cold stream inlet section at 27.5 °C and with a mass flow rate of 5.77×10^{-4} kg s^{-1}, while the hot stream enters in the heat exchanger at 463.4 °C and with a mass flow rate of about 6.79×10^{-3} kg s^{-1}. The thermophysical properties of the cold and hot streams are related with the mixture composition from the mixer and off-gas burner, respectively.

The reformer is composed by a cylindrical catalyst block (along which the reforming reactions take place) located in between two conical tubes. The catalyst block corresponds to a ceramic (cordierite) honeycomb monolith with square-shaped cells (600 cpsi) onto the surfaces of which the catalytic active particles are dispersed. For three-dimensional fluid flow and conjugate heat transfer simulation purposes, the symmetry characteristics of the reformer tubular geometry were taken advantage of to reduce the required computational cost. Therefore, only 1/8 of the total reformer cross sectional area, *i.e.*, only a 45° longitudinal slice of the entire reformer geometry was considered for simulation. Fig. 9(b) shows several features of the mesh considered for simulations. The mesh is composed by polyhedral cells with a prismatic layer on the wall of the fluid region to account for boundary layer development. A particular refinement was applied in the catalyst monolith region. The overall conformal mesh is composed by approximately 1.4 million cells. In this study, methane was considered the fuel. A temperature equal to 350 °C, an air to fuel equivalence ratio (λ) of 0.31 and a total volumetric fuel flow rate of 2 NL min^{-1} were considered as the operating condition for the reformer.

The burner is composed by two concentric metal pipes of different lengths, forming a two-stage combustion chamber. The fuel mixture enters through the inner pipe, whereas the air stream from the fuel cell cathode enters in the outer pipe through a tangential placed tube. Drilled holes in the inner pipe allow the passage of air from the outer to the inner pipe, in order to fed the first combustion chamber with oxidizer. A refined polyhedral mesh with a prismatic layer on the walls and extrusions both at the inlet and outlet was used. Special refinement care was considered for the first chamber holes and in the inner pipe (flame region). The conformal mesh for the off-gas burner presented in Fig. 9(c) comprises approximately a total of 4 million cells. The anode off-gas and cathode air streams enter in the burner at 761 °C and 690 °C, respectively. The fuel mixture has a total mass flow rate of about 2.863×10^{-4} kg s^{-1} and is composed by 0.43% and 2.6% on a mass basis of H_2 and CO, respectively.

4.3. Integrated components framework

At the simulation of integrated components level, the ventilated room is considered along with the whole μ–CHP unit, except the internal regions of the unit components. Figs. 10(a) and (b) show several features of the mesh considered for simulation in the air region along two orthogonal planes, and on the external surfaces of the unit and unit interior main components, respectively. A refined polyhedral mesh with a prismatic layer on the walls of the unit external panels and internal components was considered. A conformal mesh was ensured at the interfaces between regions described by different physics. The overall mesh is composed by a total of 2.5 million cells.

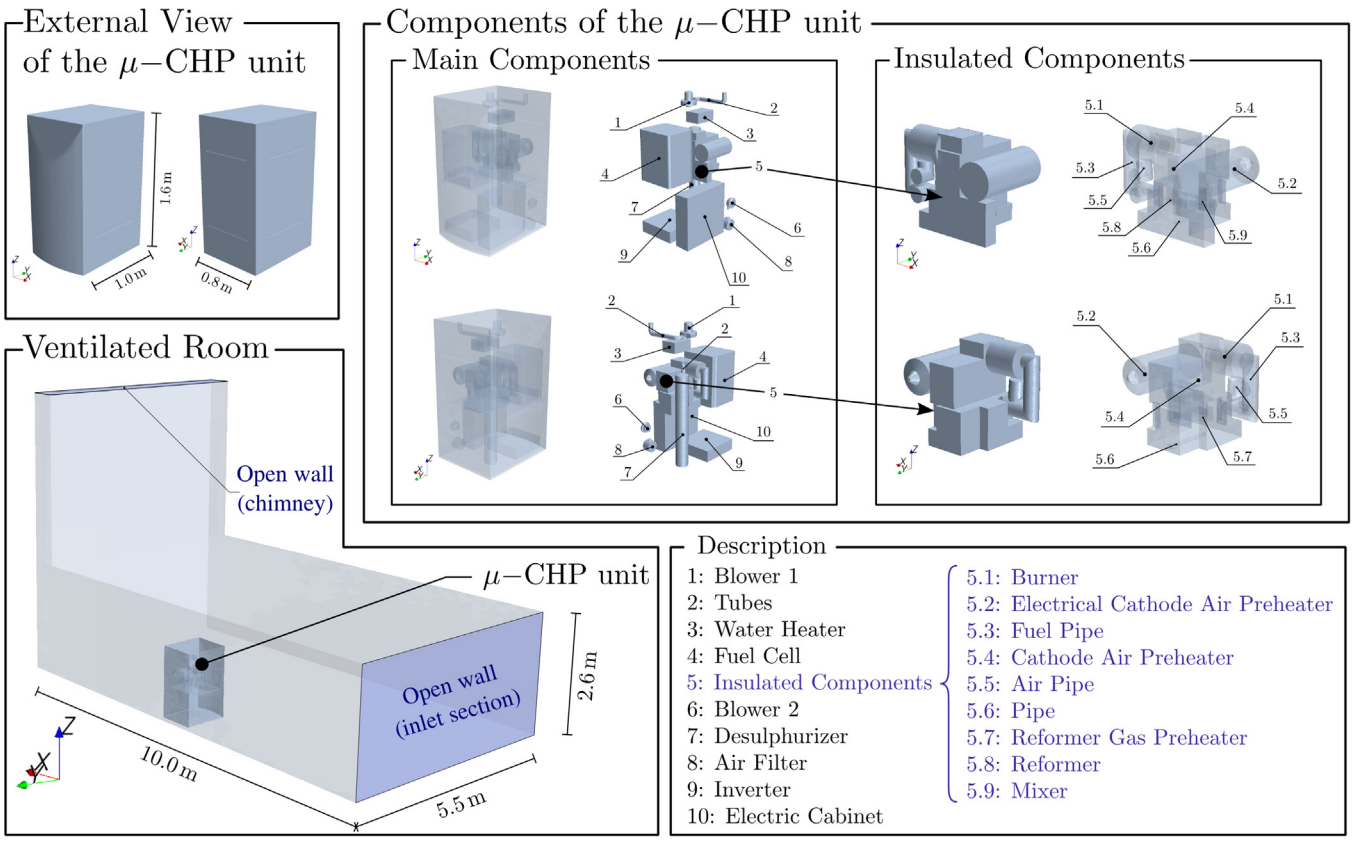

Fig. 8. Geometric definitions and internal components of the μ–CHP unit.

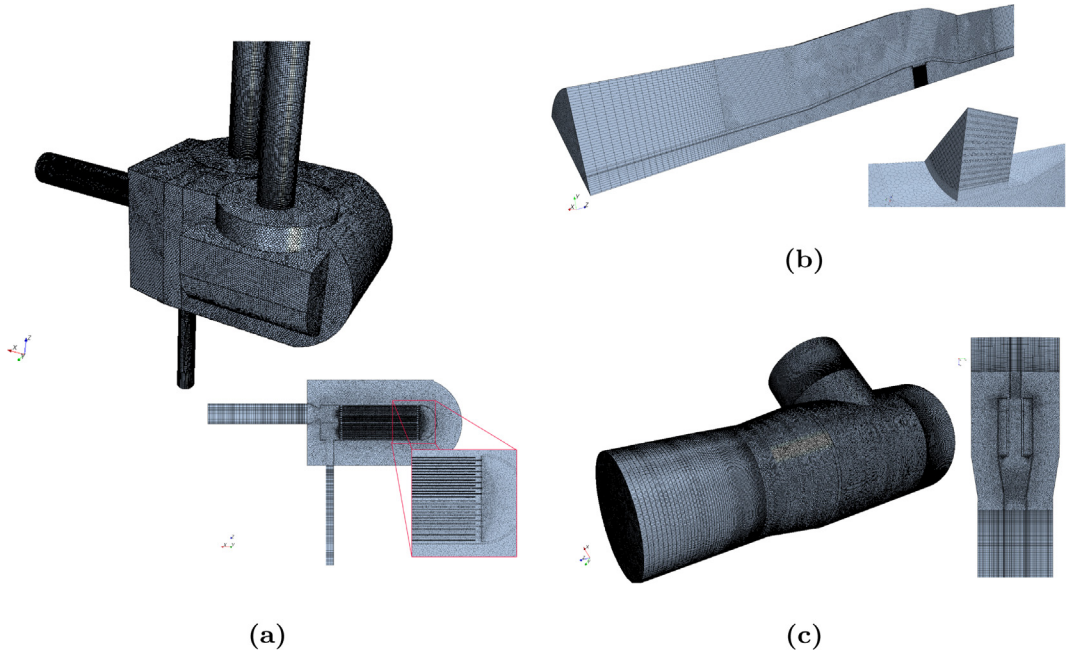

Fig. 9. Mesh representation for the unit components considered in the simulation of segregated components set: (a) reformer gas preheater; (b) reformer; (c) burner.

In accordance with the proposed methodology, the heat release from critical components considered at the simulation of segregated components level is iteratively updated on the simulation of integrated components framework. For components that were not considered for full (single) simulations, an iteration-independent boundary condition is required on their physical boundaries. Table 1 lists the boundary conditions applied for all components comprising the μ–CHP unit. These conditions were considered based on the components operation for the current unit working regime [32].

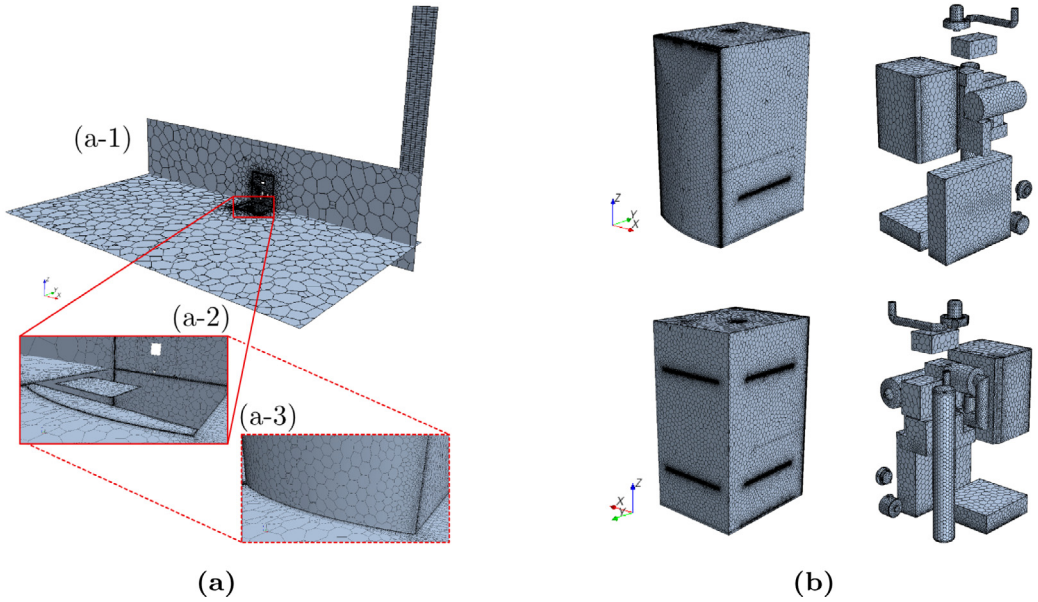

Fig. 10. Mesh geometry for the simulation of integrated components: (a) surrounding air in two orthogonal plane sections (ventilated room (a-1); close view at the unit without and with external panels (a-2) and (a-3), respectively); (b) unit external panels and interior main components.

At the inlet section of the ventilated room where the unit is installed, a specific air velocity (normal to the inlet section) and temperature are imposed. The velocity magnitude was determined equal to 0.01 m s^{-1}, considering a suitable air renewal rate in the room, and a constant air temperature at the room inlet section equal to 20 °C was considered. The room walls (floor, ceiling, lateral walls) are considered adiabatic, no-slip and impermeable boundaries. The generated heat due to the unit operation is rejected from the room through the chimney by convection.

4.4. Numerical models

The numerical solution for the boundary value problems defined previously was achieved applying the tools provided in the software package STAR-CCM+. The ideal gas law was considered as the equation of state for each fluid phase region. The segregated flow and segregated fluid temperature models were applied for the reformer gas preheater, reforming reactor and for the simulation of integrated components. The segregated flow and segregated fluid enthalpy models were applied for the off-gas burner. The SST $k-\omega$ turbulence model was taken into account for closure of the Reynolds-Averaged Navier-Stokes equations considered for the reformer gas preheater and for the off-gas burner. A multicomponent mixture description was regarded for the fluid regions of the reformer gas preheater, reformer and burner. Along the reformer, the conversion of the fresh feedstock mixture into synthesis gas was evaluated through user defined functions, based on an extensive data set for catalyst characterization carried out through a 1D single-channel heterogeneous model [33,34]. The non-premixed combustion of the fuel along the anode off-gas burner was taken into account through the PPDF reacting model. The segregated solid energy model was employed for the evaluation of the temperature in the solid regions. Microtherm MPS was the insulating material applied around the insulated components. A high temperature resistant stainless steel was considered for the reformer, reformer gas preheater, and off-gas burner housings. A thermal conductivity equal to 0.0245, 20.0, 3.0, and 15.1 W m^{-1} K^{-1} was applied for the Microtherm MPS insulating material, metallic support structures, honeycomb catalyst bed, and stainless steel, respectively.

Table 1
Boundary conditions applied for all unit components (see Fig. 8 to locate each component within the unit).

	Component	Boundary Condition
	1: Blower 1	Adiabatic surface
	2: Tubes	Adiabatic surface
	3: Water heater	$T = 300.00$ °C
	4: Fuel cell	$q'' = 118.77$ W m^{-2}
5: Insulated components	5.1: Burner	q'' iteratively computed
	5.2: E. cathode air preheater	$T = 650.00$ °C
	5.3: Fuel pipe	$T = 761.00$ °C
	5.4: Cathode air preheater	$q'' = 190.09$ W m^{-2}
	5.5: Air pipe	$T = 690.00$ °C
	5.6: Pipe	Adiabatic surface
	5.7: Reformer gas preheater	q'' iteratively computed
	5.8: Reformer	q'' iteratively computed
	5.9: Mixer	Adiabatic surface
	6: Blower 2	Adiabatic surface
	7: Desulphurizer	Adiabatic surface
	8: Air filter	Adiabatic surface
	9: Inverter	$q'' = 77.21$ W m^{-2}
	10: Electric cabinet	$q'' = 44.29$ W m^{-2}

4.5. Results

During the methodology initialization step, a constant overall heat transfer coefficient equal to 10, 25 and 40 W m^{-2} K^{-1} was considered for the reformer gas preheater, reformer and off-gas burner, respectively. These initial (coarse) estimates were considered based on the fluid flow characteristics expected in the vicinity of each component. For all components, the assigned reference temperature was equal to 293 K. The addressed reference temperature combined with the high stream temperatures and with the exothermal nature for the thermo-chemical processes occurring in the components anticipates an heat release all around the components boundaries.

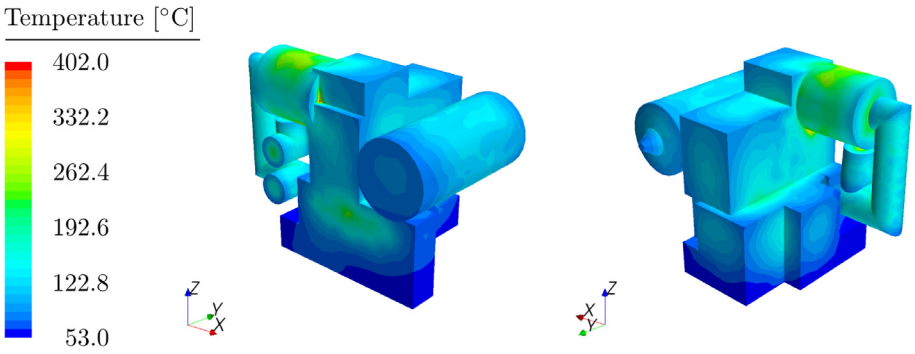

Fig. 11. Temperature on the external surface of the insulated block.

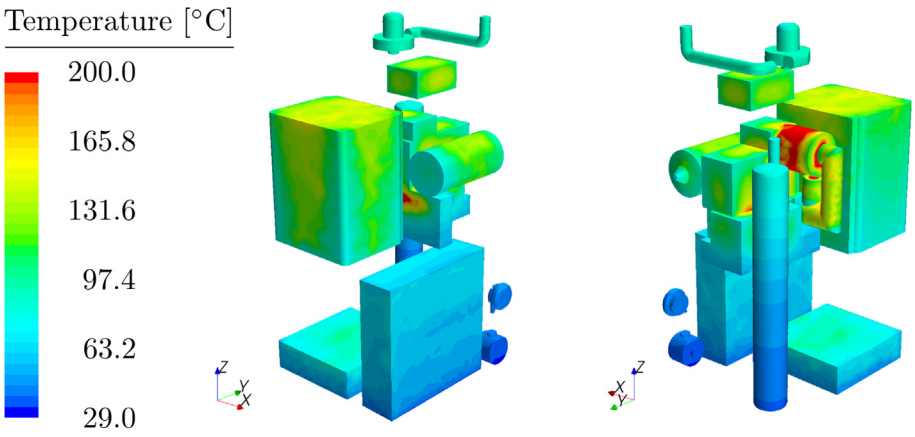

Fig. 12. Temperature on the external surface of the unit main components.

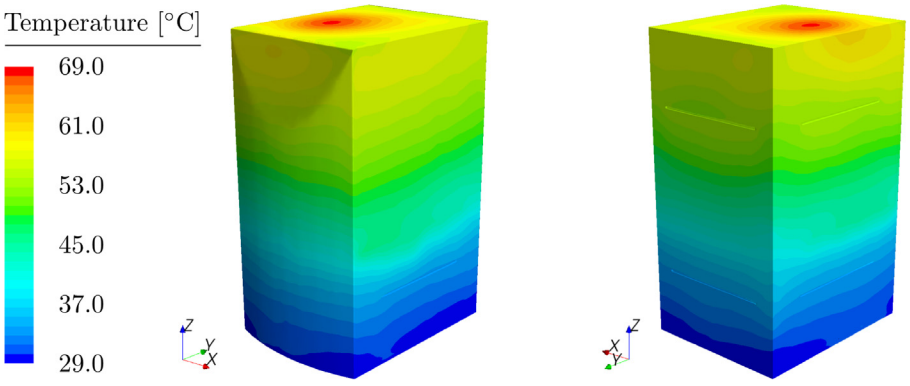

Fig. 13. Temperature on the unit external panels.

An iteration termination tolerance of 1% was considered for all components during the iterative procedure. This tolerance was achieved within three iterations. The fast convergence is in full agreement with the methodology performance observed in the verification procedure (Section 3), since the three components simulated individually do not receive energy from the surrounding system due to their location within the unit, which is coherent with the provided estimates for the initialization stage. At the end of the iterative procedure, a total heat release equal to 23.53, 28.96 and 58.40 W was calculated for the reformer gas preheater, the reformer and the off-gas burner, respectively.

Fig. 11 shows the temperature on the external surface of the insulated components. The insulation morphology and thickness around the off-gas burner constitute a critical issue since the maximum temperatures on external surface of the insulated components are related with the burner operation. The external insulation surface around the lateral walls of the burner reaches temperatures up to 257 °C. Nevertheless, the most problematic hot-spots driven by the burner activity are located on the interface between the burner insulation and the insulation that involves the cathode air preheater and the reformer gas preheater, where temperatures up to 402 and 329 °C are observed. The high exothermicity related with the H_2 and CO total oxidation reactions carried out within the burner, together with insulation imperfections around the burner installation site is responsible for a higher heat release value observed for the burner operation in relation to the heat release from the remaining components.

Fig. 12 presents the temperature on the external surface of the components inside the unit. Components located at the bottom of the unit are at a lower temperature than the components located in

the upper regions. The insulation surface around the burner is the region with the highest temperatures inside the unit. On the upper surface of the fuel cell a maximum temperature of about 160 °C is registered.

Fig. 13 shows the results for the temperature on the external panels of the unit. In general, the temperature of the panels increases from the bottom to the top of the unit. The maximum temperature in the unit external panels is observed in the upper panel (about 69 °C). This hot-spot in the unit upper panel is mainly attributed to the high heat release from the burner and fuel cell stack. For the conditions considered in this study to the μ–CHP plant operation, a decrease in the temperatures on the unit external panels can be attained by increasing the insulation thickness and improving the insulation shape around the burner installation site. In particular, a special effort should be ascribed to minimize the insulation geometrical defects, namely at the interface between the insulation that surrounds the burner and the insulation that encloses the cathode air preheater and the reformer gas preheater, where critical hot-spots are observed. As suggested in the literature [35], an alternative (or additional) measure for decreasing the temperatures of the external panels would be the application of an hot-box compartment in order to encase the most critical heat dissipative components, namely the insulated block and the fuel cell stack.

5. Conclusions

A robust methodology for thermal analysis of complex multi-component systems was proposed. The methodology decomposes the global problem into two sets of simulations. An iterative two-way procedure for coupling both simulation realms was defined in such a way that one set of simulations provides the boundary conditions for the other set. Besides promoting an increase in the convergence rate of the overall numerical solution, the current methodology can be applied for thermal management studies with the additional advantage of avoiding the tedious and labor-intensive effort related with CAD modeling and mesh generation of the whole system, whenever an improved component design is to be integrated in the system or the components location in the system is modified. For a particular system with different boundary conditions, the methodology was successfully verified against the results of the full simulation approach. The methodology was thereafter applied for a comprehensive thermal analysis study of a fuel cell based μ–CHP plant developed for providing electricity and thermal energy at a domestic level. The application of the methodology, considering a specific operating condition for the μ–CHP plant, enabled the determination of the temperature distribution within the unit and on the unit external panels. Critical hot-spots (up to about 400 °C) were observed on the external surface of the unit internal components. At the external unit panels a maximum temperature of about 69 °C was registered. A minimization of these hot-spots, as well as an approach to an adiabatic regime of operation for the critical components can be attained by increasing the insulation thickness and improving the insulation distribution.

Acknowledgements

This work was partially supported by the European Commission within the 7th Framework Program (Grant No. 260105) and by LAETA-FCT EMS/50022.

References

[1] M.T. Zhang, M.M. Jovanović, F.C. Lee, Design and analysis of thermal management for high-power-density converters in sealed enclosures, Applied Power Electronics Conference and Exposition, 1997. APEC'97 Conference Proceedings 1997, Twelfth Annual, vol. 1, IEEE, 1997, pp. 405–412.
[2] P. Cova, N. Delmonte, F. Giuliani, M. Citterio, S. Latorre, M. Lazzaroni, A. Lanza, Thermal optimization of water heat sink for power converters with tight thermal constraints, Microelectron. Reliab. 53 (9–11) (2013) 1760–1765.
[3] N. Nieto, L. Díaz, J. Gastelurrutia, F. Blanco, J.C. Ramos, A. Rivas, Novel thermal management system design methodology for power lithium-ion battery, J. Power Sources 272 (2014) 291–302.
[4] T. Wang, K.J. Tseng, J. Zhao, Z. Wei, Thermal investigation of lithium-ion battery module with different cell arrangement structures and forced air-cooling strategies, Appl. Energy 134 (2014) 229–238.
[5] A. Boglietti, A. Cavagnino, D. Staton, M. Shanel, M. Mueller, C. Mejuto, Evolution and modern approaches for thermal analysis of electrical machines, IEEE Trans. Ind. Electron. 56 (3) (2009) 871–882.
[6] A. Christensen, S. Graham, Thermal effects in packaging high power light emitting diode arrays, Appl. Therm. Eng. 29 (2–3) (2009) 364–371.
[7] C.J.M. Lasance, A. Poppe, Thermal Management for LED Applications, Springer, 2014.
[8] K.B. Abdelmlek, Z. Araoud, R. Ghnay, K. Abderrazak, K. Charrada, G. Zissis, Effect of thermal conduction path deficiency on thermal properties of LEDs package, Appl. Therm. Eng. 102 (2016) 251–260.
[9] Z. Luo, H. Cho, X. Luo, K. Cho, System thermal analysis for mobile phone, Appl. Therm. Eng. 28 (14–15) (2008) 1889–1895.
[10] Y. Tomizawa, K. Sasaki, A. Kuroda, R. Takeda, Y. Kaito, Experimental and numerical study on phase change material (PCM) for thermal management of mobile devices, Appl. Therm. Eng. 98 (2016) 320–329.
[11] S.C. Pang, M.A. Kalam, H.H. Masjuki, M.A. Hazrat, A review on air flow and coolant flow circuit in vehicles' cooling system, Int. J. Heat Mass Transf. 55 (23–24) (2012) 6295–6306.
[12] M. Khaled, M. Ramadan, H. El-Hage, A. Elmarakbi, F. Harambat, H. Peerhossaini, Review of underhood aerothermal management: towards vehicle simplified models, Appl. Therm. Eng. 73 (1) (2014) 842–858.
[13] M. Behnia, L. Maguire, G. Morrison, Cooling problems and thermal issues in high power electronics – a multi faceted design approach, in: Proceedings of the 5th International Conference on Thermal and Mechanical Simulation and Experiments in Microelectronics and Microsystems, 2004. EuroSimE 2004, IEEE, 2004, pp. 519–526.
[14] W. Nakayama, Heat in computers: applied heat transfer in information technology, J. Heat Transf. 136 (1) (2014) 013001.
[15] L. Maguire, W. Nakayama, M. Behnia, Y. Kondo, A CFD study on the effect of shrinking box size on cooling airflows in compact electronic equipment – The case of portable projection display equipment, Heat Transf. Eng. 29 (2) (2008) 188–197.
[16] E.P. Weidmann, T. Binner, H. Reister, Experimental and numerical investigations of thermal soak, SAE Int. J. Mater. Manuf. 1 (1) (2009) 145–153.
[17] S. Mao, Z. Feng, E.E. Michaelides, Off-highway heavy-duty truck under-hood thermal analysis, Appl. Therm. Eng. 30 (13) (2010) 1726–1733.
[18] M. Franchetta, T.G. Bancroft, K.O. Suen, Fast transient simulation of vehicle underhood in heat soak, Tech. Rep. 2006-01-1606, SAE Technical Paper, 2006.
[19] I. Bayraktar, Computational simulation methods for vehicle thermal management, Appl. Therm. Eng. 36 (2012) 325–329.
[20] V. Kumar, S. Kapoor, G. Arora, S.K. Saha, P. Dutta, A combined CFD and flow network modeling approach for vehicle underhood air flow and thermal analysis, Tech. Rep. 2009-01-1150, SAE Technical Paper, 2009.
[21] H. Park, Numerical assessment of liquid cooling system for power electronics in fuel cell electric vehicles, Int. J. Heat Mass Transf. 73 (2014) 511–520.
[22] M. De Paepe, P. D'Herdt, D. Mertens, Micro-CHP systems for residential applications, Energy Convers. Manage. 47 (18–19) (2006) 3435–3446.
[23] H.I. Onovwiona, V.I. Ugursal, Residential cogeneration systems: review of the current technology, Renew. Sustain. Energy Rev. 10 (5) (2006) 389–431.
[24] A. Choudhury, H. Chandra, A. Arora, Application of solid oxide fuel cell technology for power generation A review, Renew. Sustain. Energy Rev. 20 (2013) 430–442.
[25] R.P. O'Hayre, S.-W. Cha, W.G. Colella, F.B. Prinz, Fuel Cell fundamentals, John Wiley & Sons, New York, 2006.
[26] H. Ren, W. Gao, Economic and environmental evaluation of micro CHP systems with different operating modes for residential buildings in japan, Energy Build. 42 (6) (2010) 853–861.
[27] T. Elmer, M. Worall, S. Wu, S.B. Riffat, Emission and economic performance assessment of a solid oxide fuel cell micro-combined heat and power system in a domestic building, Appl. Therm. Eng. 90 (2015) 1082–1089.
[28] V. Liso, A.C. Olesen, M.P. Nielsen, S.K. Kær, Performance comparison between partial oxidation and methane steam reforming processes for solid oxide fuel cell (SOFC) micro combined heat and power (CHP) system, Energy 36 (7) (2011) 4216–4226.
[29] C. Ulloa, P. Eguía, J.L. Miguez, J. Porteiro, J.M. Pousada-Carballo, A. Cacabelos, Feasibility of using a Stirling engine-based micro-CHP to provide heat and electricity to a recreational sailing boat in different European ports, Appl. Therm. Eng. 59 (1–2) (2013) 414–424.
[30] T. Pfeifer, L. Nousch, D. Lieftink, S. Modena, System design and process layout for a SOFC micro-CHP unit with reduced operating temperatures, Int. J. Hydrogen Energy 38 (1) (2013) 431–439.
[31] L.F. Fuentes-Cortés, A. Ávila-Hernández, M. Serna-González, J.M. Ponce-Ortega, Optimal design of CHP systems for housing complexes involving weather and electric market variations, Appl. Therm. Eng. 90 (2015) 895–906.

[32] I. Frenzel, A. Loukou, D. Trimis, F. Schroeter, L. Mir, R. Marin, B. Egilegor, J. Manzanedo, G. Raju, M. de Bruijne, Development of an SOFC based micro-CHP system in the framework of the European project FC-DISTRICT, Energy Proc. 28 (2012) 170–181.
[33] J.E.P. Navalho, I. Frenzel, A. Loukou, J.M.C. Pereira, D. Trimis, J.C.F. Pereira, Catalytic partial oxidation of methane rich mixtures in non-adiabatic monolith reactors, Int. J. Hydrogen Energy 38 (17) (2013) 6989–7006.
[34] J.E.P. Navalho, J.M.C. Pereira, J.C.F. Pereira, Conical-shaped foam reactors for catalytic partial oxidation applications, Int. J. Hydrogen Energy 39 (8) (2014) 3666–3680.
[35] P. Holtappels, H. Mehling, S. Roehlich, S.S. Liebermann, U. Stimming, SOFC system operating strategies for mobile applications, Fuel Cells 5 (4) (2005) 499–508.